

Performance of Induction Motor Drive by Using Modular Multilevel Converter With Battery Energy Sources

T.Lakshman Kumar¹, P.Siva Krishna² M.Tech

Brahmaiah College Of Engineering Electrical and Electronics Engineering North Rajupalem,kovur-524137

Email: kumar.forhk@gmail.com

Abstract— This paper presents a control scheme for the Modular Multilevel Converter (MMC) to drive a variable-speed AC machine, especially focusing on improving dynamic performance. Theoretically, the energy balance in the MMC cell capacitors is prone to be unstable at start-up and at low frequency operations. Additionally, the MMC topology essentially requires advanced control strategies to balance energy and suppress the voltage pulsation of each cell capacitor. This paper proposes a control strategy for the robust dynamic response of MMC even at zero output frequency employing leg offset voltage injection. The leg offset voltage for balancing the arm energy is produced by direct calculation without the circulating current control loop controller. Thanks to the highly dynamic leg offset voltage from direct calculation and not conventional circulating current controller, the dynamic performance of the MMC at low speeds has conspicuously improved. The AC machine has been driven from standstill to rated speed without excessive cell capacitor voltage ripples utilizing this proposed strategy. The simulation and experimental results verify that stable operation is guaranteed down to less than 2 % of the rated speed under 40% step load torque disturbance.

Index Terms— arm energy balancing, dynamic performance, inner circulating current control, modular multilevel converter, motor drive

NOMENCLATURE

Superscript ‘*’	reference value.
Superscript ‘~’	low frequency component.
Superscript ‘^’	high frequency component.
x -phase	representation of one of the u , v , or w phases.
r_{so}	leg offset voltage of x -phase leg.
r_{sn}	common mode voltage.
i_{so}	circulating current of x -phase leg.
ω_s	three-phase output frequency.
R	resistance of arm inductor.
L	inductance of arm inductor.
C_{ce11}	capacitance of DC capacitor in a sub-module cell.
E_{sP}	upper arm energy in x -phase leg.
E_{sN}	lower arm energy in x -phase leg.
r_{sPi}^c	i^{th} cell capacitor voltage in upper arm in x -phase.
r_{sNi}^c	i^{th} cell capacitor voltage in lower arm in x -phase

I. INTRODUCTION

A Modular Multilevel Converter (MMC) with focus on high-power medium voltage AC motor drives is presented

[1]-[10]. The use of the MMC makes it possible to save bulky reactive components in a medium-voltage motor drive application such as a line-transformer, harmonic filter, and DC-link reactor. Compared to conventional medium voltage source converters, the MMC has a modular structure made up of identical converter cells. Because it can easily provide higher number of voltage level for medium voltage applications, the quality of the output voltage waveform is better. Also, because of the modular structure it has advantages such as easy maintenance and assembly.

Fig. 1 shows the circuit configuration of an MMC. This topology needs to be controlled by extra balancing strategies. As shown in Fig. 1, since the upper and lower arm currents flow through cells in each arm, the corresponding arm currents cause fundamental periodic pulsations of cell capacitor voltages. The voltage pulsation of each cell’s capacitor is mostly affected by the output phase current and output frequency. Theoretically, the magnitude of the cell voltage fluctuation is proportional to magnitude of the output phase current and inversely proportional to operating frequency [6]. For this reason, special effort is demanded to drive the AC machine through MMC, which requires considerable starting torque and low speed steady state operation. In recent studies of [7]-[9] and [16], the principles and algorithms for AC motor drives with the MMC have been introduced. However, they did not address the actual control strategies such as changing output frequency including standstill and covering load torque disturbance.

The energy balancing control is one of the main issues of an MMC system. In many literatures [6]-[10], the energy balancing controls of an MMC that uses circulating current control and modulation scheme has been introduced. The leg offset voltage is used to regulate the circulating current and has little effect on AC and DC terminal voltages. The conventional balancing controls need the circulating current controller that produces the leg offset voltage reference from the input of circulating current references using the proportional and integral (PI) or the proportional and resonant (PR) controller. The performance of the circulating current controller has detrimental effects on the dynamics and complexity of the balancing control. Therefore, in order to improve the balancing performance by increasing bandwidth of the balancing controller, this paper proposes a balancing control method without the circulating current controller. Therefore, in the view point of capacitor voltage balancing, the leg offset voltage can be directly obtained with no phase delay due to the circulating current controller. So, the bandwidth of balancing controller based on the direct voltage injection method can be extended more than that based on the circulating current

controller. In addition, the difference between the cell voltages can be reduced faster. As a result, from the perspective of the control dynamics and control complexity, the proposed leg offset voltage injection method is better and simpler than the conventional circulating current injection method. Furthermore, the injecting frequency of leg offset voltage injection method can be increased more than that of current injection method, because of the extended bandwidth of the proposed method. So, owing to the high frequency injection with the proposed method, the fluctuation of cell capacitor voltage can be minimized compared to circulating current injection method.

The goal of this paper is to propose a control strategy of the entire frequency range operation including standstill for variable speed AC motor drive. The proposed method reduces the control performance degradation of the MMC when the load torque abruptly changes. The control scheme introduces two operation modes. One is a low frequency mode for start-up and low speed operation, and the other is a normal frequency mode from medium to higher speed operation. The strategy in the low frequency mode exploits leg offset voltage and common mode voltage with the high frequency component to suppress the cell capacitor voltage ripple. The square wave voltage is used as the leg offset voltage, which shows that the circulating current peak is reduced when compared to sinusoidal waveform of the voltage [7]. A switchover tactic between two operation modes is described to drive the AC machine in the overall speed region.

To prove the effectiveness of the proposed control strategies, a 12kV 24MVA MMC based adjustable motor drive system was designed by using the PSIM software. The simulation results could offer the feasibility and advantage of the devised method for high power medium voltage drives with MMC. And then, experiments for variable-speed AC motor drives by a 10kVA prototype MMC emulating fans, blowers, or pump drive system were performed to verify the feasibility of the proposed balancing strategy. The experiments were conducted for comparing features of the sinusoidal and square wave leg offset voltage. The stable operation at 1Hz, which is less than 2% of the rated speed, is shown under an abrupt step

load torque disturbance from 0% to 40% in order to demonstrate the dynamic performance. The experimental

results show that all control strategies was well incorporated in the variable-speed AC motor drive system with a load where the torque varies in proportional to the square of the speed, like fans, blowers, or pumps.

II. CONFIGURATION AND BASIC PRINCIPLE OF

THE MMC

Fig. 1(a) shows the circuit configuration of the MMC. The three-phase MMC is composed of three legs and each leg has two arms and two arm inductors. Each arm has cascaded N -identical half-bridge circuit based cells, and each cell consists of one DC capacitor and two active

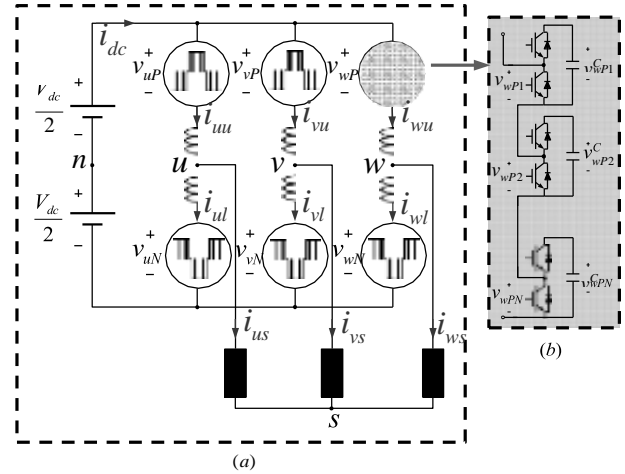


Fig. 1. Circuit configuration of the MMC.

in Fig. 1(b) in detail. In Fig. 1(a), i_{su} and i_{sl} are the upper and lower arm currents, respectively, and i_{sx} is the output phase current where 'x' represents the u, r, or w phase. The output phase current, i_{sx} , and circulating current, i_{so} , are calculated from the upper and lower arm currents described in (1)-(2). Therefore, the arm currents can be deduced as (3)-(4), according to the decoupled control scheme in [8], [11].

$$i_{xs} = i_{xu} - i_{xl}. \quad (1)$$

$$i_{xo} = (i_{xu} + i_{xl})/2. \quad (2)$$

$$i_{xu} = \frac{1}{2} i_{xs} + i_{xo}. \quad (3)$$

$$i_{xl} = -\frac{1}{2} i_{xs} + i_{xo}. \quad (4)$$

The leg offset voltage, r_{so} , produces a circulating current defined as (5), where R and L stand for the resistance and inductance of an arm inductor when all arm inductors in MMC are assumed to be identical. From the voltage relationships along the x-phase loop, the upper and lower arm voltage references are denoted as (6) and (7), respectively, where V_{dc} is the DC-link voltage, and r_{sP} and r_{sN} are the upper and lower arm voltage respectively. The common mode voltage, r_{sn} , is the

voltage difference between nodes 's' and 'n', and r_{ss} is the phase voltage, which is $r_{ss} = V_m \cos(m_s t)$. A detailed mathematical description of the relationships in an MMC is given in [10].

$$v_{xo} = \left(R + L \frac{d}{dt} \right) i_{xo}. \quad (5)$$

$$v_{xP}^* = \frac{V_{dc}}{2} - v_{xs}^* - v_{sn}^* - v_{xo}^*. \quad (6)$$

$$v_{xN}^* = \frac{V_{dc}}{2} + v_{xs}^* + v_{sn}^* - v_{xo}^*. \quad (7)$$

switching devices. The cascaded cell modules are depicted

the instantaneous power of each arm in the x -phase can be deduced as (8)-(9). These two equations must be considered to understand of the proposed balancing control.

$$P_{xP} = v_{xP}^* i_{xu} = \left(\frac{V_{dc}}{2} - v_{xs}^* - v_{sn}^* - v_{xo}^* \right) \left(\frac{1}{2} i_{xs} + i_{xo} \right). \quad (8)$$

$$P_{xN} = v_{xN}^* i_{xl} = \left(\frac{V_{dc}}{2} + v_{xs}^* + v_{sn}^* - v_{xo}^* \right) \left(-\frac{1}{2} i_{xs} + i_{xo} \right). \quad (9)$$

In addition, the upper and lower arm energy can be calculated by (10) and (11), respectively. Each arm energy is the sum of the cell capacitor energies in the corresponding arm at x-phase leg.

$$E_{xP} = \frac{1}{2} C_{cell} \sum_{i=1}^N (v_{xPi}^C)^2. \quad (10)$$

$$E_{xN} = \frac{1}{2} C_{cell} \sum_{i=1}^N (v_{xNi}^C)^2. \quad (11)$$

(17)

III. PROPOSED BALANCING CONTROL SCHEME

A. Start-up and Low Frequency Mode

The capacitor power difference between the upper and lower arm, which is derived as (12) from (8) and (9), affects the cell capacitor voltage balance of the arms. The first two terms on the right-hand side in (12), $0.5V_{dc}i_{xs} - 2r_{sn}i_{so}$ have considerable DC or very low frequency components. Thus, when the output frequency is DC or very low, the voltage difference between the arms will diverge due to this low frequency term.

$$P_{xP} - P_{xN} = 0.5V_{dc}i_{xs} - 2v_{xs}^*i_{xo} - 2v_{sn}^*i_{xo} - v_{xo}^*i_{xs}. \quad (12)$$

To balance the power difference between arms, a control strategy exploiting the common mode voltage, r_{sn} , was used in this paper. The common mode voltage can be regarded as an additional degree of freedom for controllability since the common mode voltage does not affect the line-to-line output voltage. It is natural to select the frequency of the common mode voltage as a high frequency to minimize the cell capacitor voltage fluctuations. In addition, since the circulating current, i_{so} , is also a controllable element that does not affect the output phase current, a high frequency component can be superimposed on the circulating current. Hence, the third

term on the right-hand side in (12), $2r_{sn}i_{so}$ can be

used

to balance the power of arms with the high frequency components in r_{sn} and i_{so} . For convenience, the low and high frequency elements can be segregated from i_{so} and r_{sn} as (13) and (14), where “~” and “^” refer to the

low and high frequency components, respectively.

To nullify the low frequency as in(15) the low frequency component of $2\hat{v}_{sn}\hat{i}_{so}$ should be controlled thus v_{sn} and i_{sn} should be regulated as the same frequency same high frequency to make the power term of $2\hat{v}_{sn}\hat{i}_{so}$ have DC or low frequency component.

In the case of the sinusoidal leg offset voltage injection method, \hat{r}_{sn}^* and \hat{r}_{so}^* can be defined as (16)-(17), and m_h refers to the angular speed of the high frequency component, V_{sn} for the effective value of common mode voltage and the magnitude of high frequency leg offset voltage which may have dc and several low frequency components

$$\hat{v}_{sn}^* = \sqrt{2}V_{sn}\cos(\omega_h t). \quad (16)$$

$$\hat{v}_{xo}^* = \hat{V}_{xo}\cos(\omega_h t + \phi). \quad (17)$$

The phase angle ϕ in (17) between the leg offset voltage and circulating current is derived from (18) to make the circulating current synchronize with the common mode voltage.

$$\phi = \arctan\left(\frac{\omega_h L}{R}\right). \quad (18)$$

in general, $m_h L$ is much larger than R , because the frequency of injecting voltage is quite high. However, if the frequency is not high enough and the arm resistance cannot be ignored, the arm impedance parameters would need to be identified. For identification, at the system commissioning stage, the non-interacting leg offset voltage can be injected into the arm, and the circulating current could be fed back as in (5). Consequently, the phase angle between the leg offset voltage and the circulating current in (18) can be obtained. Under the assumption of $R \ll m_h L$, ϕ is approximately $\pi/2$. From (5) and (16)-(17), the low frequency component of the power associated with the common mode voltage and the circulating current can be derived as (19) using the leg offset voltage, where p represents a differential operator.

$$\begin{aligned} 2\hat{v}_{sn}\hat{i}_{xo}|_{low\ freq.} &\approx 2\hat{v}_{sn}\frac{v_{xo}}{pL}|_{low\ freq.} \\ &= \frac{2\sqrt{2}V_{sn}\hat{V}_{xo}}{\omega_h L}\cos(\omega_h t)\sin\left(\omega_h t + \frac{\pi}{2}\right)|_{low\ freq.} \\ &= \frac{2\sqrt{2}V_{sn}\hat{V}_{xo}}{\omega_h L}\left(\frac{1}{2}\sin\left(\frac{\pi}{2}\right) + \frac{1}{2}\sin\left(2\omega_h t + \frac{\pi}{2}\right)\right)|_{low\ freq.} \\ &= \frac{\sqrt{2}V_{sn}\hat{V}_{xo}}{\omega_h L}. \end{aligned} \quad (19)$$

$$i_{xo} = \tilde{i}_{xo} + \hat{i}_{xo}. \quad (13)$$

$$\tilde{v}_{sn} = \hat{v}_{sn}. \quad (14)$$

The power difference between the upper and lower arms can be rearranged from (12)-(14), and then, the low frequency power component can be extracted as in (15). Here, the power difference should be controlled as null.

$$\begin{aligned} & (P_{xP} - P_{xN})|_{low\ freq.} \\ & \approx 0.5V_{dc}i_{xs} - 2v_{xs}^*i_{xo} - 2\hat{v}_{sn}^*\hat{i}_{xo}|_{low\ freq.} = 0. \end{aligned} \quad (15)$$

And then, $2\hat{v}_{sn}^*\hat{i}_{xo}$ (15) can be substituted with (19). The magnitude of high frequency leg offset voltage, \tilde{V}_{xo} , can be calculated as (20).

$$\begin{aligned} \frac{\sqrt{2}V_{sn}\tilde{V}_{xo}}{\omega_h L} & \approx \frac{1}{2}V_{dc}i_{xs} - 2v_{xs}^*i_{xo} \\ \Leftrightarrow \tilde{V}_{xo} & \approx \frac{\omega_h L}{\sqrt{2}V_{sn}} \left(\frac{1}{2}V_{dc}i_{xs} - 2v_{xs}^*i_{xo} \right). \end{aligned} \quad (20)$$

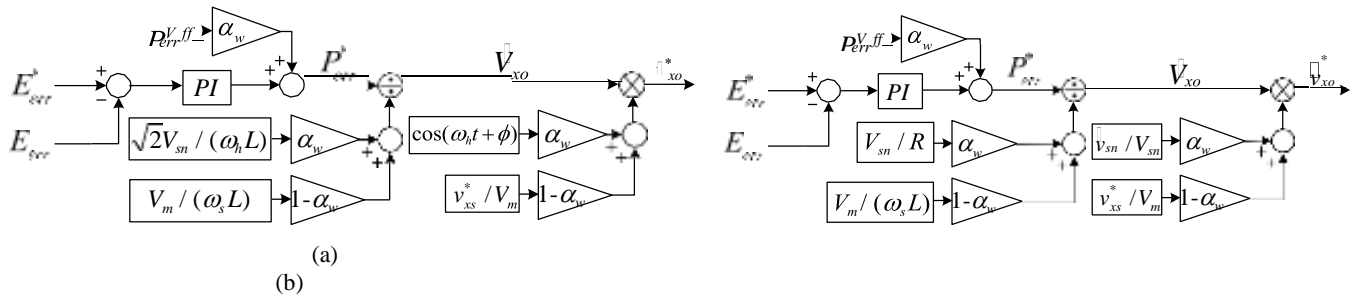


Fig. 2. Proposed control scheme for variable-speed drives: (a) sinusoidal wave voltage injection method, (b) square wave voltage injection method. α_w is weighting factor for switchover, which is described in section C of chapter III.

In the case that the sinusoidal wave voltage is injected to both the common mode and the leg offset voltage, the balancing control strategy is depicted as a block diagram in Fig. 2(a). E_{err} is the energy difference between the upper and lower arms as in (21). E_{err} is the reference of energy difference and should be set as null to keep the balance of the arm energies.

$$E_{err} = E_{xp} - E_{xn} = \frac{1}{2} C_{coll} \left\{ \sum_{t=1}^N (v_{xt}^c)^2 - \sum_{t=1}^N (v_{xn}^c)^2 \right\} \quad (21)$$

$P_{err}^{V,ff}$ in Fig. 2(a) can be derived as (22) by (20).

$$P_{err}^{V,ff} = \frac{1}{s} V_{dc} i_{xs} - 2V_{xs}^* i_{xo} \quad (22)$$

In the case of the square leg offset voltage injection, on the other hand, the square wave voltage can be injected to both the common mode and the leg offset voltage, as shown in Fig. 2(b). In this case, \hat{v}_{sn} can be defined by (23), and f_h stands for the frequency of the injected high frequency voltage.

$$\hat{v}_{sn}^* = \begin{cases} -V_{sn} & (0 \leq t < \frac{1}{2f_h}) \\ V_{sn} & (\frac{1}{2f_h} \leq t < \frac{1}{f_h}) \end{cases} \quad (23)$$

under the assumption that the arm resistance, R , is dominant during each given quasi steady half period,

$1/(2f_h)$, \hat{v}_{so} can be approximated as (24) from (5), (15), and (23).

$$\hat{v}_{xo}^* \approx \begin{cases} -\frac{R}{2V_{sn}} (\frac{1}{2} V_{dc} i_{xs} - 2v_{xs}^* i_{xo}) & (0 \leq t < \frac{1}{2f_h}) \\ \frac{R}{2V_{sn}} (\frac{1}{2} V_{dc} i_{xs} - 2v_{xs}^* i_{xo}) & (\frac{1}{2f_h} \leq t < \frac{1}{f_h}) \end{cases} \quad (24)$$

$P_{err}^{V,ff}$ in Fig. 2(b) can also be derived from (22) by using (24) similarly with the case of sinusoidal wave.

B. Normal Frequency Mode

Since the output frequency is high enough in the normal frequency mode, the voltage fluctuation of the cell capacitor is tolerable. In this mode, the circulating current is controlled to have only DC component to minimize the

Practical MMC systems may have an inherent unbalance due to slight asymmetries in cells, structural errors, and other issues. In normal frequency mode, therefore, it should be performed just to eliminate the

inevitable small DC unbalances. The balancing can be

achieved by using the circulating current as $2v_{xs}^* i_{xo}$ in (12). By regulating the leg offset voltage for circulating current to have fundamental frequency component, this DC unbalance can be suppressed.

C. Switchover between Two Model



Fig. 3. The relationship between operating frequency and weighting factor.

As mentioned previously, as the high frequency components of the common mode and leg offset voltage

are only injected in low operating frequency modes, the leg offset voltage reference changes depending on the output frequency of MMC. A switchover tactic between the low and high frequency modes shown in Fig. 3 is devised by the weighting factor, α_w . And, this factor is applied to the switchover of the balancing control scheme shown in Fig. 2. In addition, the tactic would have the hysteresis band to prevent chattering in the vicinity of the switchover frequency, f_{cut} .

conduction loss caused by the additional circulating current. As the operation frequency increases, meanwhile, the margin of the common mode voltage decreases. Hence, the common mode voltage is less available for balancing

$$P_{xp} + P_{xn} \approx V_{dc} i_{xo} - 2v_{xo}^* i_{xo} - v_{xs}^* i_{xs} - \hat{v}_{sn}^* i_{xs} \quad (25)$$

OVERALL CONTROL SCHEME FOR ENTIRE FREQUENCY OPERATION

Fig. 4 shows the overall controller for the entire frequency operation from standstill to normal control.

frequency mode. Firstly, the averaging controller carries out regulating the leg power, which is the difference between DC-link input power and AC output power. The leg power is calculated as (25) by adding (8) and (9).

* * *

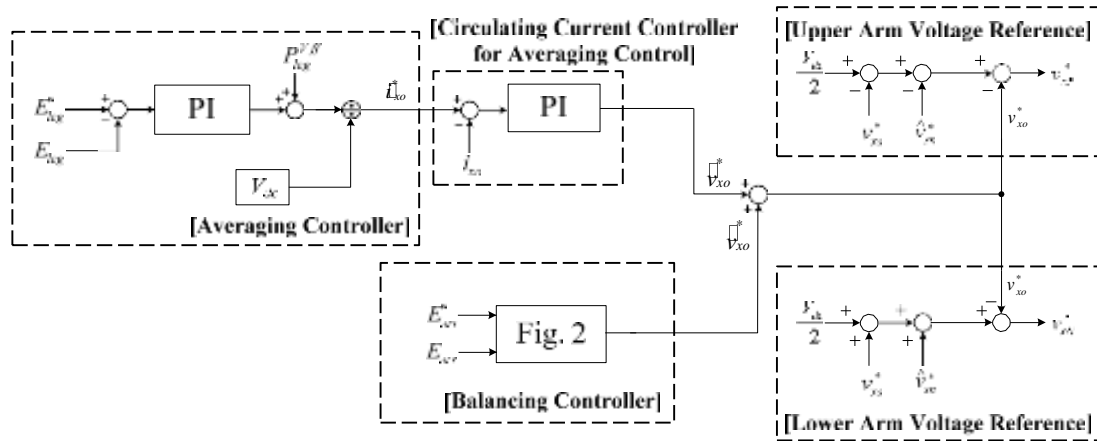


Fig. 4. Proposed overall control scheme for variable-speed drives.

Because the low frequency power component in (25) should be nullified as in (26), the controller output has DC and 2nd order harmonic frequency components as described in (27).

$$P_{xP} + P_{xN}|_{low\ freq.} \approx V_{dc} \tilde{i}_{xo} - v_{xs}^* i_{xs} = 0. \quad (26)$$

$$\tilde{i}_{xo} = v_{xs}^* i_{xs} / V_{dc}. \quad (27)$$

E_{1Eg} is the energy of the leg, and it can be calculated

and the cell capacitance is 6000 μ F. The Nearest Level as (28). E_{1eg} is the reference energy of the leg as (29),

where r_c is the reference value of cell capacitor voltage, V_{dc}/N .

$$E_{leg} = E_{xP} + E_{xN} = \frac{1}{2} C_{cell} \left\{ \sum_{i=1}^N (v_{xPi}^c)^2 + \sum_{i=1}^N (v_{xNi}^c)^2 \right\} \quad (28)$$

$$E_{leg}^* = \frac{1}{2} \frac{C_{cell}}{2N} 4N^2 V_c^2 = NC_{cell} V_c^2. \quad (29)$$

The feed-forwarding power term, P_{leg}^{Vff} , can be derived as $v_{xs}^* i_{xs}$ from (27). Therefore, the proportional and integral controller can simply be adopted as the circulating current controller for the averaging control. The details about the averaging controller are described in [10].

Meanwhile, the balancing controller can be chosen between two schemes in Fig. 2 which are, namely, the sinusoidal and the square wave voltage injections. As shown in Fig. 4, the balancing controller directly makes the leg offset voltage without the circulating current controller to eliminate the energy difference between upper and lower arms. By reason of this fact, the balancing controller has a wider bandwidth, and can achieve a better transient response compared to the control scheme based on the inner circulating current regulation loop.

Finally, the upper and lower arm voltage references are synthesized as (6) and (7), which are composed of r_{ss}^*

from the output of phase current controller, r_{so} from the averaging and balancing controller, and the injected

24MVA MMChosen implemented by using the time-domain simulation program, PSIM. The number of cells in each arm, N, equals 20. Thus the system with 120 cells was simulated. Each cell capacitor voltage is controlled as

Modulation (NLM) is applied to generate the arm voltage references and reduce the switching loss of MMC [15].

The cell voltage sorting algorithm is applied to the cell

voltage balancing [14]. The parameters used in the simulation are listed in Table I.

TABLE I. CIRCUIT PARAMETERS OF THE SIMULATIONS

Description	Abbreviation	Value
Rated apparent power	S_{MMC}	24MVA
Rated line-to-line rms voltage	V_s	8.32kV
Rated line frequency	f_s	60Hz
DC-link voltage	V_{dc}	12kV
Cell capacitance	C_{cell}	6000 μ F
Arm inductance	L	4mH

It is assumed that the 21-level MMC system drives a 20MW 20-pole Permanent Magnet Synchronous Machine (PMSM) with adjustable mechanical load. The PMSM parameters are summarized in Table II.

TABLE II. CIRCUIT PARAMETERS OF THE SIMULATIONS

Description	Abbreviation	Value
Rated active power	P_{PMSM}	20MW
Rated line-to-line rms voltage	V_{rated}	8kV
Rated rotational speed	ω_{rm}^{rated}	360r/min
Pole pair number	pp	10

From the simulation results, the devised method can be

common mode voltage of \hat{f}^* .

IV. SIMULATION RESULTS

To verify the effectiveness of the proposed control strategy, an adjustable speed drive system based on 12kV

applied to high power medium voltage adjustable drive system based on MMC. From the dynamic comparison between circulating current injection with the inner current loop and the proposed leg offset voltage injection method, it can be concluded that the proposed method might be an

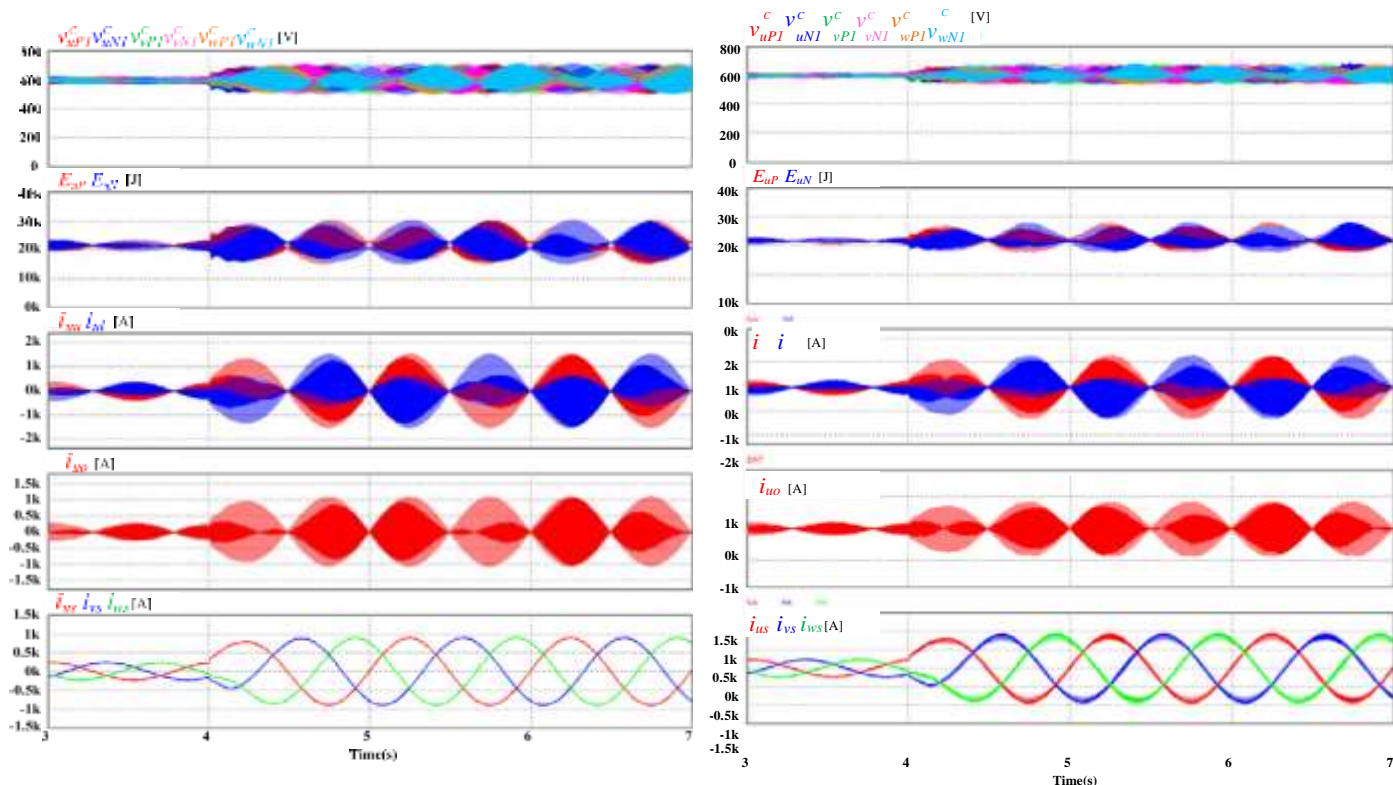


Fig. 5. The simulation waveform when applying the proposed leg offset voltage injection method with 6r/min speed and step load torque from 10% to 40% of the rated torque: (a) sinusoidal waveform offset voltage injection, (b) square waveform offset voltage injection.

acceptable solution for high power medium voltage drives based on MMC under requirements of considerable torque disturbance and steady state operation down to a few percent of the rated frequency.

Fig. 5 shows the low frequency operation at 1Hz (6r/min, less than 2% of the rated frequency) with an abrupt step load torque from 50kN-m (10%) to 200kN-m (40%) at 4s. Fig. 5(a) shows the simulation result of the sinusoidal wave leg offset voltage method, and Fig. 5(b) shows that of the square wave leg offset voltage method. The high frequency (100Hz) voltage is used to balance the arm in low the frequency mode in both sinusoidal and square wave cases. Before 4s, the PMSM is controlled to be 6r/min with 10% load torque. At the time point 4s, the 40% load torque is abruptly applied to the PMSM. Regardless of the impact of step load torque, MMC systems with both sinusoidal and square wave cases have successfully kept the stable operation. Meanwhile, comparing the waveforms between Fig. 5(a) and Fig. 5(b), the square waveform method can save the magnitude of the circulating current. Additionally, it has better balancing ability than the sinusoidal waveform method, from the view of the u-phase upper and lower cell capacitor voltage fluctuations.

Meanwhile, In Fig. 6, the simulation results with the conventional circulating current injection method based on the inner current regulating loop is shown. All operating conditions are identical to those in Fig. 5 except for the magnitude of the step load torque. For fair comparison between the conventional current injection and proposed leg offset voltage injection methods, the bandwidth for the balancing controller of the two methods is set as the same, and the frequency of the injected component was also set as the same, 100Hz. The magnitude of the step load torque applied at the conventional current injection method is 36% of the rated

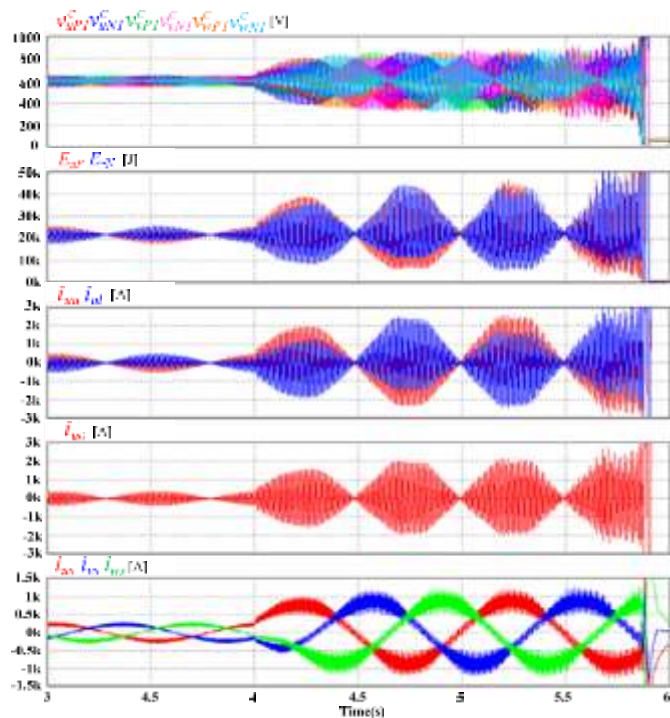


Fig. 6. The simulation waveform when applying the conventional circulating current injection method with 6r/min speed and step load torque from 10% to 36% of the rated torque.

torque, which is less than the proposed method test in Fig. 5. As shown in Fig. 6, the system based on the conventional method becomes unstable and stalls in a moment at the end. After the abrupt step load torque is applied at 4s, the cell capacitor voltage fluctuations are larger than the fluctuations when using the leg offset voltage injection method in Fig. 5.

3-PHASE INDUCTION MOTOR

This section covers 3-phase asynchronous motors, the most commonly used motors for driving machinery. The use of this type of motor has become the norm in a large number of applications because of its numerous advantages: it is standardized, rugged, easy to maintain and use, and inexpensive

Stator

This is the altered piece of the engine. A cast iron or light combination casing encompasses a ring of dainty overlays (around 0.5 mm thick) made of silicon steel. The covers are protected from each other by oxidation or a protecting varnish. The "overlay" of the attractive circuit diminishes misfortunes by means of hysteresis and whirlpool streams. The overlays have openings in them for holding the stator windings that create the pivoting field (three windings for a 3-stage engine). Every winding is comprised of various loops. The way these curls are joined to each other characterizes the quantity of sets of posts of the engine, and accordingly the pace of turn.

Rotor

This is the moving piece of the engine. Like the attractive circuit of the stator, it is comprised of a heap of dainty covers protected from each other, framing a keyed barrel on the engine shaft. Two distinct innovations can be utilized for this part, which isolate offbeat engines into two unmistakable families: those with a "squirrel confine" rotor and those with an injury rotowhic are alluded to as "slip-ring".

Three-phase motor rotating field

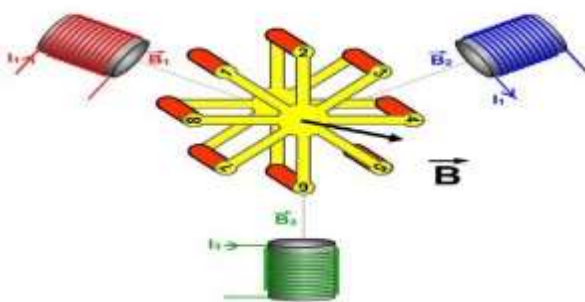


Fig.2.4:-3-phase squirrel cage induction motor

2.4.1 PRINCIPLE AND WORKING

At the point when 3 stage supply is given to the engine, the subsequent current produces an attractive flux "Ø". Due to the exchanging succession of 3 stage current in R, Y and B, the created flux pivots around the rotor conductor As showed by Faraday's law which communicates that – "an emf influenced in any close circuit is a direct result of the rate of advancement of appealing flux through the circuit". Emf is provoked in the Copper bar and on account of this, present streams in the rotor. The course of rotor can be given by Lenz law which

communicates that – "the orientation of actuated current will be in the converse of the development bringing

on it" Here the relative speed between the turning flux and static rotor conductor is the explanation behind current time; subsequently the rotor will rotate in the same going to abatement the reason i.e. the relative rate, subsequently turning the rotor of the insincerity motor.

POWER SUPPLY:

The stator is connected with a 3-stage aerating and cooling power supply. In the going hand in hand with blueprint organize An is joined with stage An of the power supply. Stage B and C would similarly be connected with stages B and C of the power supply indivassociated with stages B and C of the force supply individual

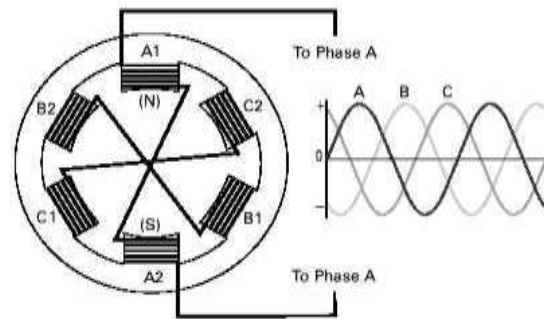


Fig.2.4.1:-power supply to motor

Stage windings (A, B, and C) are put 120° separated. In this sample, a second arrangement of three-stage windings is introduced. The quantity of shafts is dictated by how often a stage winding shows up. In this sample, every stage winding seems two times. This is a two-shaft stator. In the event that every stage winding seemed four times it would be a four-shaft stator



At the point when air conditioning voltage is connected to the stator, current courses through the windings. The attractive field grew in a stage twisting relies on upon the bearing of current move through that winding. The accompanying outline is utilized here for clarification just. It will be utilized as a part of the following couple of outlines to show how a pivoting attractive field is created. It accept that a positive current stream in the A1, B1 and C1 windings bring about a north post.

V. EXPERIMENTAL RESULTS

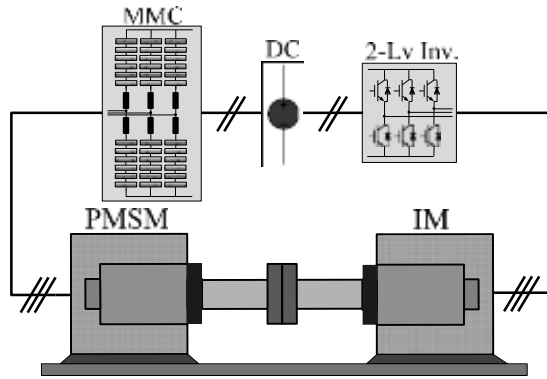


Fig. 7. Experimental setup with 300V 10kVA prototype MMC system.

The proposed control strategy is validated by the 300V 10kVA reduced scale prototype MMC shown in Fig. 7. The number of cells in each arm, N , is 6, so there are a total of 36 cells used for the three-phase system. Each cell capacitor voltage is controlled at 50V and each cell includes two power MOSFET switches which have 100V/120A ratings. The level-shifted Phase Disposition PWM (PD-PWM) generates arm voltage references [12]-[13], and the voltage balancing of cell capacitors in each arm is achieved by sorting algorithms [14]. The carrier

frequency of each cell is set as 2kHz and the DC link

capacitance of each cell is 4400 μ F. The parameters of the system under test are summarized in Table III.

TABLE III. CIRCUIT PARAMETERS OF THE EXPERIMENTS

Description	Abbreviation	Value
Rated active power	P_{PMSM}	11kW
Rated line-to-line rms voltage	V_{rated}	200V
Rated rms line current	I_{rated}	58.6A
Rated rotational speed	ω_{rm}^{rated}	1750r/min
Pole pair number	pp	4

A. The Sinusoidal Leg Offset Voltage Injection

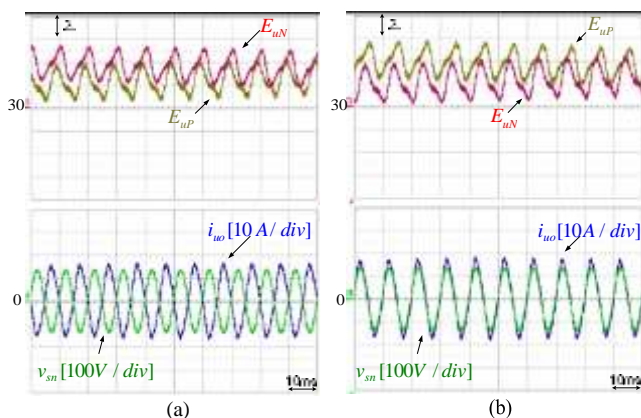


Fig. 8. The experimental waveform of the low frequency mode operation at 1Hz output frequency with the sinusoidal leg offset voltage: (a) negative energy difference and (b) positive energy difference.

Fig. 8 shows the waveform in condition of the low frequency operation mode at 1Hz output frequency with 20% load torque. The injected leg offset voltage is the 100Hz sinusoidal wave. Fig. 6 shows the upper and lower arm energy of the u -phase calculated from (10)-(11). The difference between the upper and lower arm is counterbalanced by $r_{sn}^* \hat{s}_{so}$. When the energy difference, $E_{uP} - E_{uN}$, is negative, the high frequency circulating current and offset voltage are controlled 180 degrees out of phase as shown in Fig. 8(a). In contrast, when the difference is positive, the circulating current and offset voltages are controlled to be in phase in Fig. 8(b).

B. The Square Leg Offset Voltage Injection

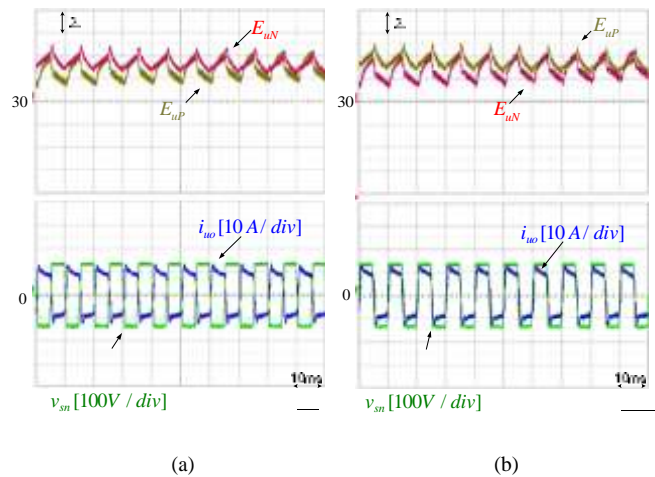


Fig. 9. The experimental waveform of the low frequency mode with 1Hz output frequency when using the square leg offset voltage: (a) negative energy difference and (b) positive energy difference.

Fig. 9 is the waveform of the low frequency operation mode at 1Hz output frequency with 20% load torque. The balancing control is performed by using the 100Hz square wave leg offset voltage. Fig. 9 shows the energy of the upper and lower arm in the u -phase leg. The energy difference is counterbalanced by $r_{sn}^* \hat{i}_{so}$ as in the

preceding sinusoidal wave case. In this experiment, the trapezoidal wave was used instead of square wave, because the output voltage might have unwanted high frequency distortion due to the nonlinearities of cells such as dead time. If the energy difference, $E_{uP} - E_{uN}$, is negative, the high frequency circulating current and offset voltage are controlled to be 180 degree out of phase as shown in Fig. 9(a). In contrast, when the difference is positive, the circulating current and offset voltages are controlled to be in phase as in Fig. 9(b).

As described in [7], the square wave can shave the peak of circulating current by 50%. However, because of trapezoidal waveform in this experiment the peak value of circulating current (i_{so}) is smaller by 37% than that of the sinusoidal voltage case.

C. Dynamic Comparison between Circulating Current Injection and Leg Offset Voltage Injection

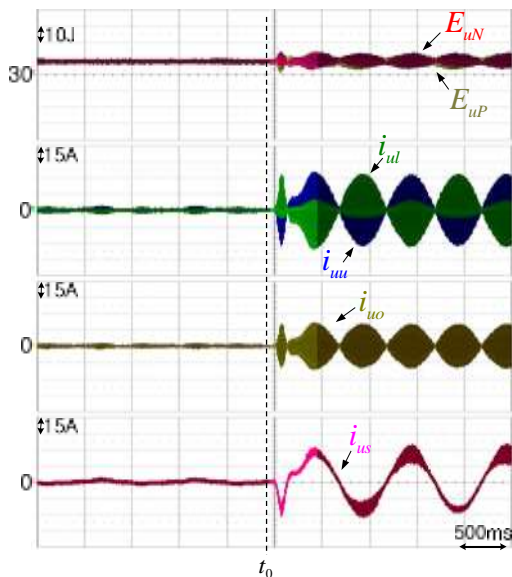


Fig. 10. The experimental waveform when applying the leg offset voltage injection method with $m_{rm} = 15r/min$ and 40% step load torque at t_0 .

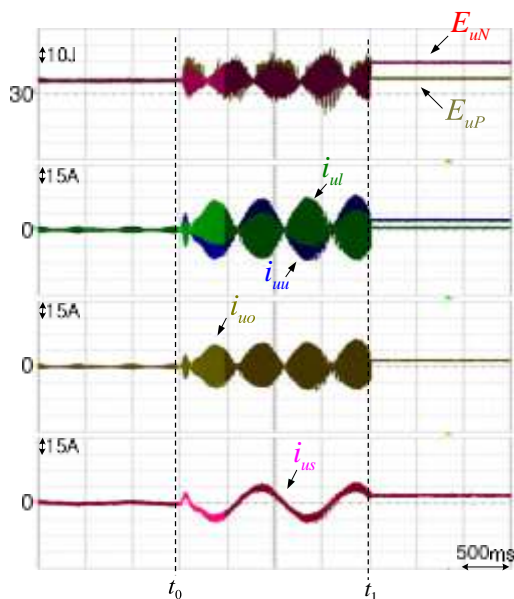


Fig. 11. The experimental waveform when applying the conventional circulating current injection method with $m_{rm} = 15r/min$ and 20% step load torque at t_0 .

Fig. 10 shows the low frequency operation at 1Hz (15r/min, less than 2% of the rated speed) when an abrupt step load torque was applied from 0N-m to 24N-m (40%) at t_0 . The square wave leg offset voltage is injected in 100Hz for the arm balancing at this experimental result. Before time point, t_0 , the PMSM was controlled to be 15r/min without load torque. At the time point, t_0 , the 40% step load torque is applied through torque control of the IM. After t_0 , the upper and lower arm energy fluctuations became larger because of the significant

output phase current by the step load torque. Furthermore, the transient response in the circulating current becomes well regulated within 300ms after the step variation in the torque. Regardless of the impact of load torque, PMSM has successfully kept the speed showing reasonable low speed performance. This result confirms that the proposed controller achieves a good transient response.

In contrast, the conventional circulating current injection method with the inner current regulating loop has been applied to balancing control as shown in Fig. 11. For fair comparison between the conventional current injection and the proposed leg offset voltage injection methods, the bandwidth for two methods was set as the same, and the frequency of the injected component was also set as the same, 100Hz. However, the magnitude of the step load torque applied at the conventional current injection method was half of the proposed method in Fig.

10. As shown in Fig. 11, the system became unstable and stalled at the end despite the lower external load torque. After the abrupt step load torque was applied at t_0 , the fluctuations of the upper and lower arm energies were larger than that when using leg offset voltage injection method in Fig. 10. Finally, the balancing controller could not achieve system balance, and the overvoltage trip of cell capacitor occurred and the system stalled at the time point of t_1 .

And it can be concluded that the leg offset voltage injection method has better disturbance load torque rejection performance.

D. The Operation from Standstill to Normal Frequency Mode

Finally, Fig. 12 shows the entire operation from standstill to the normal frequency mode, 1000r/min. In order to conduct the switchover operation in a practical application of variable speed drive such as fans, blowers, or pumps, the load torque was emulated with IM in proportional to the square of the speed. Furthermore, the start-up torque of 24N-m (40%) is included in the torque profile ($T_{L_profile}$). And, the phase current before t_{start} is regulated as the DC value. At the time point t_{change} , the switchover process starts, and the operating mode changes to the normal frequency operation mode. When the rotating speed (m_{rm}) is 1000r/min, the applied load torque to PMSM is 100% of the rated torque, 60N-m. As shown in Fig. 12, it has been confirmed that the proposed control strategies depicted in Fig. 4 are well implemented and incorporated properly to drive the variable speed AC machine in overall speed including standstill by the MMC.

VI. CONCLUSIONS

In this paper, a control strategy for variable-speed AC motor drives based on MMC has been presented. To overcome the difficulties of the power balance between cells and arms of MMC over wide operation speed ranges, a direct leg offset voltage injection method has been devised. Utilizing the proposed method, the ripple voltage of each cell of MMC has been kept within allowable

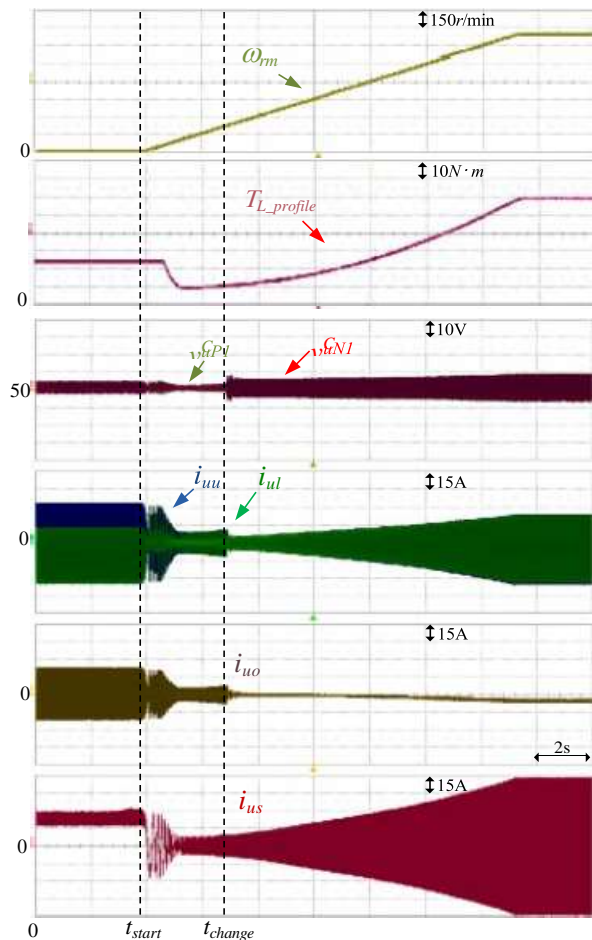


Fig. 12. Experimental waveforms in the condition of variable speed drive from starting to 1000r/min with 40% starting torque and the increasing load torque depending on rotating speed.

bounds under the sudden application of 40% of rated load torque at the extremely low frequency, 1Hz, which is less than 2% of rated frequency. Based on the simulation and experimental results, it can be noted that the control performance of the upper and lower arm energy ripple by the proposed leg offset voltage injection method is better than that by the conventional circulating current injection method with the inner loop. In addition, the variable speed AC motor drive has been proven to work based on the switchover tactic by testing the overall speed including standstill.

REFERENCES

[1] A. Lesnicar and R. Marquardt, "An innovative modular multilevel converter topology suitable for a wide power range." *Power Tech Conference Proceedings, 2003 IEEE Bologna*. Vol. 3. IEEE, 2003.

[2] M. Hiller, D. Krug, R. Sommer, and S. Rohner, "A new highly modular medium voltage converter topology for industrial drive applications." *Power Electronics and Applications, 2009. EPE'09. 13th European Conference on*. IEEE, 2009.

[3] G. P. Adam, O. Anaya-Lara, G.M. Burt, D. Telford, B. W. Williams, and J. R. McDonald, "Modular multilevel inverter: pulse width modulation and capacitor balancing technique." *IET power electronics* 3.5 (2010): 702-715.

[4] H. M. Pirouz, M. T. Bina, and K. Kanzi, "A new approach to the modulation and dc-link balancing strategy of modular multilevel

ac/ac converters." *Power Electronics and Drives Systems, 2005. PEDS 2005. International Conference on*. Vol. 2. IEEE, 2005.

[5] A. Antonopoulos, K. Ilves, L. Angquist, and H.-P. Nee, "On interaction between internal converter dynamics and current control of high-performance high-power ac motor drives with modular multilevel converters." *Energy Conversion Congress and Exposition (ECCE), 2010 IEEE*. IEEE, 2010.

[6] M. Hagiwara, K. Nishimura, and H. Akagi, "A medium-voltage motor drive with a modular multilevel PWM inverter." *Power Electronics, IEEE Transactions on* 25.7 (2010): 1786-1799.

[7] M. Hagiwara, I. Hasegawa, and H. Akagi, "Start-Up and Low-Speed Operation of an Electric Motor Driven by a Modular Multilevel Cascade Inverter," *Industry Applications, IEEE Transactions on*, vol.49, no.4, pp.1556,1565, July-Aug. 2013.

[8] J. Kolb, F. Kammerer, and M. Braun, "Straight forward vector control of the Modular Multilevel Converter for feeding three-phase machines over their complete frequency range." *IECON 2011-37th Annual Conference on IEEE Industrial Electronics Society*. IEEE, 2011.

[9] A. Antonopoulos, L. Angquist, S. Norrga, K. Ilves, and H.-P. Nee, "Modular multilevel converter ac motor drives with constant torque from zero to nominal speed." *Energy Conversion Congress and Exposition (ECCE), 2012 IEEE*. IEEE, 2012.

[10] Jae-Jung Jung, Hak-Jun Lee, and Seung-Ki Sul. "Control of the Modular Multilevel Converter for variable-speed drives." *Power Electronics, Drives and Energy Systems (PEDES), 2012 IEEE International Conference on*. IEEE, 2012.

[11] Angquist, Lennart, A. Antonopoulos, D. Siemaszko, K. Ilves, M. Vasiladiotis, and H.-P. Nee, "Inner control of modular multilevel converters-an approach using open-loop estimation of stored energy." *Power Electronics Conference (IPEC), 2010 International*. IEEE, 2010.

[12] Tengfei Wang and Yongqiang Zhu, "Analysis and comparison of multicarrier PWM schemes applied in H-bridge cascaded multilevel inverters." *Industrial Electronics and Applications (ICIEA), 2010 the 5th IEEE Conference on*. IEEE, 2010.

[13] S. Rohner, S. Bernet, M. Hiller, and R. Sommer, "Modulation, losses, and semiconductor requirements of modular multilevel converters." *Industrial Electronics, IEEE Transactions on* 57.8 (2010): 2633-2642.

AUTHORS



T.LAKSHMAN KUMAR received his B.Tech degree in Electrical and Electronics Engineering from Malineni Lakshmaiah Institute of Engineering and Technology, Ramannapalem, Nellore dist, affiliated to JNTU Ananthapur. He is currently pursuing

M.Tech power electronics in Brahmaiah college of engineering, north rajupalem, SPSR Nellore (Dist), affiliated To JNTU Ananthapur.



P.SIVA KRISHNA received his B.Tech Degree in Electrical and Electronics Engineering from Narayana engineering college, Nellore affiliated to jntu ananthapur. He received his M.Tech from sree venkataperumalu engineering college puttur,chitter dist. He has 1 years teaching experience, presently working as Professor of

EEE, Brahmaiah college of engineering Affiliated to JNTU, Anantpur. Andhra Pradesh, India